ACS APPLIED MATERIALS & INTERFACES

www.acsami.org

Research Article

Label-free Electrochemical Detection of CGG Repeats on Inkjet Printable 2D Layers of MoS_2

Narges Asefifeyzabadi,[⊥] Rana Alkhaldi,[⊥] Ahmad Z. Qamar, Adrian A. Pater, Meera Patwardhan, Keith T. Gagnon, Saikat Talapatra, and Mohtashim H. Shamsi*

Cite This: *ACS Appl. Mater. Interfaces* 2020, 12, 52156–52165

Read Online

ACCESS | Metrics & More | Article Recommendations | Supporting Information

ABSTRACT: Flexible and ultrasensitive biosensing platforms capable of detecting a large number of trinucleotide repeats (TNRs) are crucial for future technology development needed to combat a variety of genetic disorders. For example, trinucleotide CGG repeat expansions in the *FMR1* gene can cause Fragile X syndrome (FXS) and Fragile X-associated tremor/ataxia syndrome (FXTAS). Current state-of-the-art technologies to detect repeat sequences are expensive, while relying on complicated procedures, and prone to false negatives. We reasoned that two-dimensional (2D) molybdenum sulfide (MoS_2) surfaces may be useful for label-free electrochemical detection of CGG repeats due to its high affinity for guanine bases. Here, we developed a low-cost and sensitive wax-on-plastic electrochemical sensor using 2D MoS_2 ink for the detection of CGG repeats. The ink containing few-layered MoS_2 nanosheets was prepared and characterized using optical, electrical, electrochemical, and electron microscopic methods. The devices were characterized by electron microscopic and electrochemical methods. Repetitive CGG DNA was adsorbed on a MoS_2 surface in a high cationic strength environment and the electrocatalytic current of the CGG/MoS_2 interface was recorded using a soluble $Fe(CN)_6^{-3/-4}$ redox probe by differential pulse voltammetry (DPV). The dynamic range for the detection of prehybridized duplexes ranged from 1 aM to 100 nM with a 3.0 aM limit of detection. A detection range of 100 fM to 1 nM was recorded for surface hybridization events. Using this method, we were able to observe selectivity of MoS_2 for CGG repeats and distinguish nonpathogenic from disease-associated repeat lengths. The detection of CGG repeat sequences on inkjet printable 2D MoS_2 surfaces is a forward step toward developing chip-based rapid and label-free sensors for the detection of repeat expansion sequences.

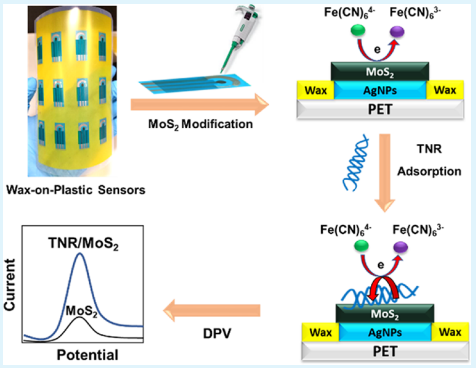

KEYWORDS: *trinucleotide repeats, DNA repeat expansions, neurodegenerative disorders, transition metal dichalcogenides, MoS_2 nanosheets, electrochemical, label-Free detection, wax-on-plastic sensors, inkjet printing*

INTRODUCTION

Expansion of CGG microsatellite repeat sequences are associated with two distinct neurological disorders, Fragile X-associated tremor/ataxia syndrome (FXTAS) and Fragile X syndrome (FXS), when expanded between 55−200 repeats or beyond 200 repeats, respectively.[1,2] Current diagnostic testing involves DNA microarray technology that relies on fluorescence labels and repeat primed PCR for signal amplification.[3] However, microarrays have critical limitations for the detection of GC-rich repeats[4−6] because polymerases do not traverse highly repetitive and GC-rich sequences efficiently.[7] Common high-throughput whole-genome sequencing technologies are typically limited to ∼150 base pair read lengths, making it difficult or impossible to map repetitive reads back to the genome.[8] Some long-read next-generation sequencing technologies can sequence across disease-associated repeat expansion sizes.[9] However, detection of microsatellite repeat expansions by these methods is costly, time consuming, and is still under development. One widely used technique, repeat-primed PCR (RP-PCR), is also frequently prone to false negatives and imprecise estimation of repeats.[10] To overcome current detection challenges while developing rapid and sensitive detection tools, electrochemical strategies have been explored previously to distinguish trinucleotide repeat (TNR) expansion sequences from shorter sequences. Electrochemical platforms generally exhibit simplicity and sensitivity for detection.[11−18] However, these electrochemical TNR detection reports heavily relied on labeling steps and expensive gold or commercial screen-printed electrodes. Thus, label-free and low-cost electrochemical sensors would further improve detection of expanded TNR sequences and help bring simple,

Received: August 19, 2020
Accepted: October 23, 2020
Published: November 5, 2020

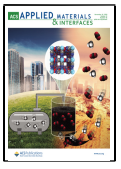

https://dx.doi.org/10.1021/acsami.0c14912
ACS Appl. Mater. Interfaces 2020, 12, 52156−52165

affordable, and effective detection methods closer to the clinic. Here, we report a label-free and low-cost electrochemical sensor based on a desktop printable wax-on-plastic chip that employs 2D molybdenum sulfide (MoS_2) electrodes to detect CGG repeats.

MoS_2 is a transition metal dichalcogenide with a 2D layer structure and comprises S−Mo−S layers stacked together through intermolecular van der Waal (vdW) forces. Recently, MoS_2-based surfaces have gained visibility for their use in DNA hybridization detectors.[19−26] This is because theoretical and experimental studies have shown that, despite having a negative charge on the surface, MoS_2 has a strong adsorption affinity for negatively charged DNA through vdW forces between the aromatic rings of nucleobases and the basal plane of MoS_2.[27,28] This also results in a higher electrocatalytic current in the presence of the negative redox probe $Fe(CN)_6^{-3/-4}$.[25] However, hybridization between complementary strands on a MoS_2 surface weakens binding affinity and results in desorption of the duplex.[21] Other reports suggest that adsorption of DNA on MoS_2 surfaces is dependent on the ionic strength of Na^+ and Mg^{2+} in solution.[29] In a solution-based study using a fluorescence readout, Liu and coworkers confirmed that the adsorption of DNA on MoS_2 can be enhanced by using the high ionic strength of Mg^{2+} due to the greater number of positive charges that can shield electrostatic repulsion between DNA and MoS_2.[24] Theoretical studies also indicated that MoS_2 has the greatest adsorption for guanine bases,[30,31] which was later experimentally confirmed.[24] Moreover, a study using a homologous sequence confirmed that longer DNA sequences may show better adsorption on MoS_2 surfaces. A well-known 2D material, graphene, has a similar structure to MoS_2 and shares some similar properties. Nevertheless, MoS_2 has some excellent properties related with transition-metal dichalcogenides, such as highly efficient fluorescence quenching. Therefore, MoS_2-based fluorescence biosensing[21,32,33] has shown better sensitivity than graphene-based methods.[34,35] For DNA detection, MoS_2 exhibits high affinity to adsorb DNA without further surface treatment or modification, which is superior to graphene.[36,37] Therefore, MoS_2 is a promising candidate for developing low-cost and sensitive DNA biosensors.

In this study, bulk MoS_2 was exfoliated by ultrasonication and converted into an inkjet printable ink in an α-terpineol medium. Due to the weak interlayer vdW interaction, it is possible to easily isolate atomically thin 2D sheets of MoS_2 layers through simple exfoliation methods.[38,39] The properties of the ink were characterized by electron microscopy, UV−visible spectroscopy, and electrical and electrochemical conductivity. Then, MoS_2-modified wax-on-plastic electrochemical sensors were fabricated by a straightforward combination of wax printing, inkjet printing, and drop casting methods. The fidelity of the devices was characterized by electron microscopic and electrochemical methods. Scheme 1 illustrates the adsorption of trinucleotide repeats (TNR) on MoS_2-modified wax-on-plastic electrochemical sensors followed by measuring the electrocatalytic current in the presence of a $Fe(CN)_6^{-3/-4}$ redox reporter using differential pulse voltammetry. The sensitivity of the sensor was tested for a prehybridized duplex, surface hybridization, repeat concentration, sequence type and length, and normal versus abnormal lengths of CGG repeats in a label-free format. We report label-free electrochemical detection of CGG repeat expansions in the FXTAS disease-associated range using a low-cost and sensitive MoS_2-based wax-on-plastic platform.

Scheme 1. Fabrication of a MoS_2-modified wax-on-plastic electrochemical sensor followed by detection of a trinucleotide repeat (TNR) on the MoS_2 surface by an electrocatalytic current response in the presence of $Fe(CN)_6^{3-/4-}$ via differential pulse voltammetry (DPV).

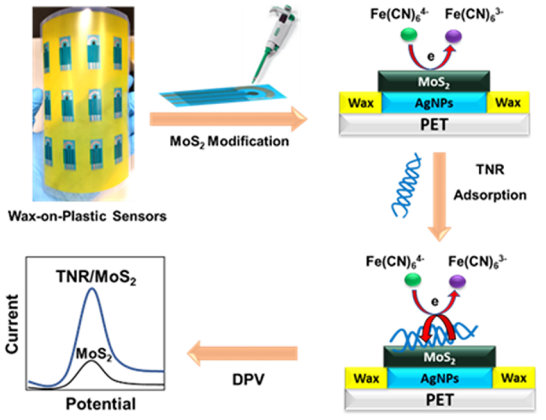

EXPERIMENTAL SECTION

Materials. All synthetic oligonucleotide sequences shown in Table S1 were purchased from Integrated DNA Technologies (U.S.A.). Longer CGG repeat DNA containing 26 and 100 units were prepared from plasmids obtained as a kind gift from Dr. Peter Todd (University of Michigan). Preparation of 26 and 100 CGG repeat expansion sequences, as well as validation by Sanger and next-generation long-read sequencing methods, is described in the Supplementary Information (Figures S7 and S8). Molybdenum disulfide (MoS_2) raw bulk powder (<2 μm, 99%), ethyl cellulose (EC) with a viscosity of 4 cP (5%) in toluene/ethanol 80:20 (lit.), 48% ethoxy, α-terpineol (90%), and tris(hydroxymethyl)aminomethane (Tris−ClO_4) were purchased from Sigma−Aldrich. Ethanol (95%), cyclohexanone, $K_4[Fe(CN)_6]$, $K_3[Fe(CN)_6]$, and phosphate-buffered saline (PBS) at pH 7.4 (10X solution) were purchased from Fisher Scientific. The holy carbon-coated grid was purchased from SPI Supplies (U.S.A.). A Xerox ColorQube 8580/DN was purchased from Xerox Inc. Polyethylene terephthalate substrate (PET), metalon silver inkjet ink (JS-B25HV), and an Epson Stylus C88$^+$ inkjet printer were obtained from Novacentrix (Austin, Texas). An electrochemical workstation CHI 660E was purchased from CHI Instruments (Austin, Texas) and used for all electrochemical measurements by coupling a commercial adaptor (product of Dropsens) obtained from Metrohm (U.S.A.). The indium tin oxide-coated substrate (ITO), 50 × 75 × 0.7 mm, R_s = 4−8 Ω, was purchased from Delta Technologies. A Fujifilm Dimatix materials printer (DMP-2800) was used for printing on the ITO substrate and purchased from Fujifilm U.S.A. A Thermo Scientific NanoDrop One spectrometer was used for UV−visible characterization of the MoS_2 ink. A Branson Ultrasonic bath (5800 model) was used for sonication. A Hitachi H-7650 transmission electron microscope operating at 60 kV and Quanta 450 FEG (FEI) at the SIU Imaging Center were used for characterization of MoS_2 ink and fabricated devices. Electrical measurements were performed using Keithley 2400-series source meters.

MoS_2 Exfoliation and Ink Formulation. Molybdenum disulfide (MoS_2) bulk powder was exfoliated using an ultrasonication bath method as reported earlier.[40,41] Briefly, 4 g of ethyl cellulose (EC) was dissolved in 200 mL of ethanol; 10 g MoS_2 bulk powder was added to this solution, and then this mixture was sonicated for 5 h. The resulting dispersion was centrifuged at 3500 rpm for 1 h. Then, 0.04 g/mL of an aqueous NaCl solution was added to the supernatant and centrifuged at 6000 rpm for 30 min. The sediment was collected by vacuum filtration followed by rinsing with water and air drying. To

https://dx.doi.org/10.1021/acsami.0c14912
ACS Appl. Mater. Interfaces 2020, 12, 52156−52165

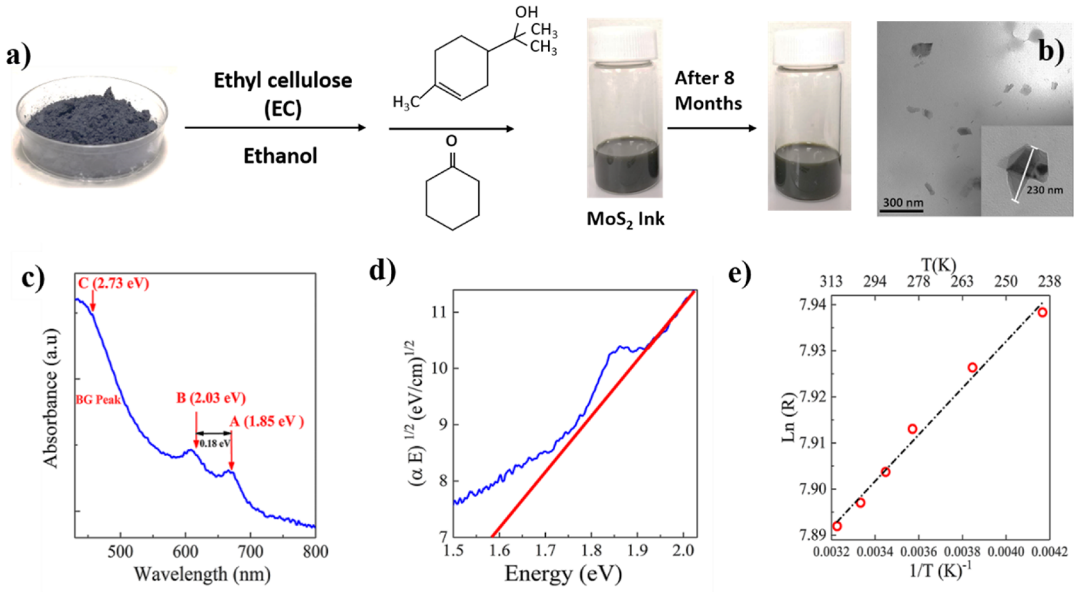

Figure 1. (a) Exfoliation and printing scheme of MoS_2. (b) TEM images of exfoliated MoS_2 nanosheets in the prepared ink. (c) UV−vis spectrum. (d) Tauc plot with linear extrapolation, giving an indirect band gap of ∼1.58 eV, an Arrhenius plot of ln*R* with T^{-1} (bottom X) and temperature (*T*) (top X) with a source voltage of 0.5 V. The dotted line is the fit obtained using the thermal activation model.

prepare the MoS_2 ink for inkjet printing, the MoS_2/EC powder was dispersed in an 85:15 cyclohexanone/terpineol mixture and sonicated for 2.5 h,[40,41] and then stored at room temperature. The final concentration of MoS_2 ink was 6% with a viscosity of 10 cp, which is required to jet from the nozzle of the Dimatix inkjet cartridge.

Characterization of MoS_2 Ink. A UV-vis spectrum scan of MoS_2 ink was taken from the 200 to 800 nm wavelength by dropping 5 μL of ink on the NanoDrop spectrometer, which was used to calculate the band gap energy of MoS_2 by making the Tauc plot from the UV−vis spectrum. Transmission electron microscopic (TEM) images of the MoS_2 nanosheets in the ink were obtained by dropping a small amount of MoS_2 ink on the holy carbon-coated grid followed by air drying before imaging.

Electrical Characterization. For electronic transport studies, the device was mounted on the cold head of the cryostat (SHI Cryogenics Group, RDK-101 D). After mounting the chip on the cold head, the chamber was evaluated to achieve high vacuum (∼10^{-5} torr) through a mechanical and turbo pump (BOC Edwards). The temperatures of the cold head were controlled by a closed cycle helium compressor (Sumitomo heavy industries Ltd., helium compressor unit, CAN-11).

Inkjet Printing of MoS_2. For electrochemical characterization, MoS_2 ink was printed on ITO substrates by using a Dimatix inkjet printer employing parameters as reported before.[41] In brief, printing of the MoS_2 ink was performed with the 10 pL inkjet nozzle plate held at 35 °C and the substrate platform held at 30 °C. The device pattern, circles with a 2 mm diameter, was designed using Inkscape (Version 0.91) software and was printed by 20 layer-printing. Following printing, thermal annealing conditions were carefully optimized similar to a previously reported study,[42] which is a crucial step to prevent oxidation of MoS_2 to MoO_3 and MoO_2 that are formed above 250 °C in air. Therefore, thermal annealing of inkjet-printed MoS_2 on the ITO substrate was performed at 300 °C in an Ar environment for 30 min.

Electrochemical Characterization of MoS_2. To study the electrochemical behavior of MoS_2 ink on the ITO substrate, cyclic voltammetry with a potential window from −0.6 to 1 V was performed at different scan rates between 50−500 mV/s in 1 mM $K_4[Fe(CN)_6]/K_3[Fe(CN)_6]$ (1:1) prepared in PBS buffer at pH 7.2. Ag/AgCl and platinum wire were used as a reference electrode and a counter electrode, respectively.

Fabrication of Wax-on-Plastic Electrochemical Devices. A three-electrode wax-on-plastic system was designed and fabricated with few changes in the previously reported procedure.[43] First, wax patterns were printed on flexible PET substrates, called wax on plastic, using a Xerox ColorQube 8580 printer. Previously, we deposited a conductive layer of AgNPs by hand painting.[43] Here, we inkjet-printed a AgNP layer on top of the wax-on-plastic patterns using an Epson Stylus C88+ inkjet printer. After washing the AgNP ink from the top of the wax layer and drying, another wax layer on the wires of each electrode was printed, which covered the wires but left the defined area of sensing electrodes and contact pads exposed. Then, 4 μL of MoS_2 ink was drop-casted on top of the working electrode followed by sintering at 120°C for 1 h in an Ar environment. The scanning electron microscope (SEM) images of the surfaces and interfaces of fabricated devices were obtained to characterize the device layers before and after sintering.

Electrochemical Study of TNR on the MoS_2 Surface. Solution hybridized double-stranded TNR was prepared by mixing equal volumes and concentrations of complementary strands in 100 μM Tris buffer, pH 8.5, containing 200 mM NaCl and 20 mM $MgCl_2$ followed by heating to their melting temperatures for 30 min and annealing at room temperature for 1 h. For electrochemical studies, 5 μL aliquots of double-stranded trinucleotide repeat (dsTNR) was dropped on MoS_2 working electrodes and incubated for 16 h at 4 °C as reported earlier.[44] For surface hybridization, 5 μL of the 1 μM probe sequence (ssCGG-8) was dropped on the working electrode and incubated as mentioned above. Then, the surface of the working electrode was washed with Tris buffer and dried with an N_2 stream. Different concentrations of complementary targets (CGG-8) were then dropped for 2 h followed by washing with buffer. Finally, differential pulse voltammetry with a potential of −0.1 to 0.2 V and an amplitude of 0.05 V was performed in 1 mM $Fe(CN)_6^{-3/-4}$ in PBS buffer (pH 7.2). The sequences and lengths of CGG TNRs are shown in Table S1.

RESULTS AND DISCUSSION

MoS_2 ink was prepared by solution-phase exfoliation of the bulk MoS_2 material (Figure 1a). Exfoliation in ethanol and stabilization in ethyl cellulose (EC) polymer provided several advantages for inkjet printing, including a high yield and low-cost ink production using an environmentally benign solvent.[40,41,45] Dispersion of dried MoS_2/EC powder in a solvent system of 85:15 v/v cyclohexanone/terpineol produced

https://dx.doi.org/10.1021/acsami.0c14912
ACS Appl. Mater. Interfaces 2020, 12, 52156−52165

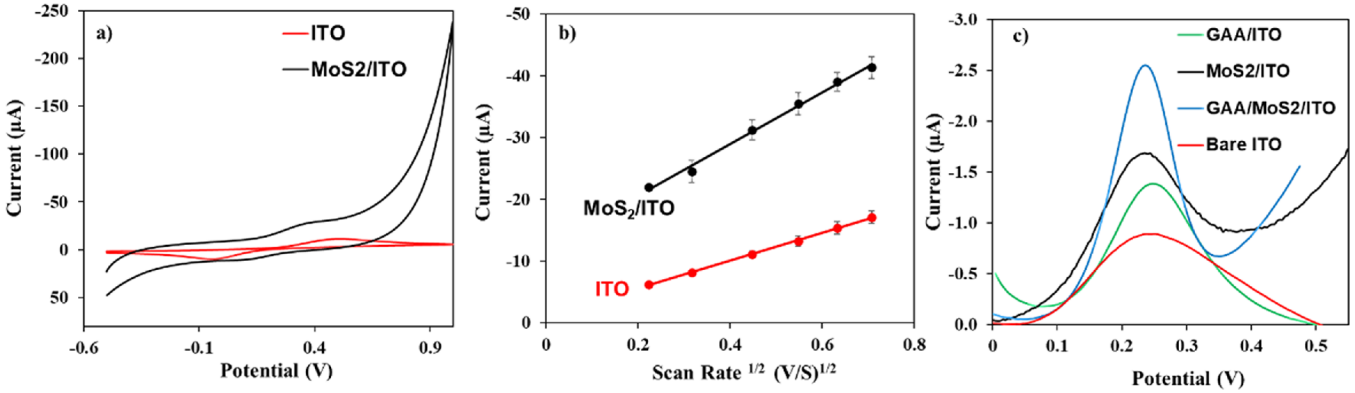

Figure 2. (a) Cyclic voltammetric curves of bare ITO (red) and inkjet-printed MoS_2 on ITO (black); (b) plot of the anodic volatmmetric current vs square root of the scan rate for bare ITO and MoS_2/ITO working electrodes. Linear equations: ITO: $y = -22.476x - 1.1022$ ($R^2 = 0.9994$) and MoS_2/ITO: $y = -41.823x + 12.244$ ($R^2 = 0.9947$). (c) Differential pulse voltammetric response of bare ITO (**0.8 μA**), GAA/ITO (**1.4 μA**), MoS_2/ITO (**1.65 μA**), and GAA/MoS_2/ITO (**2.5 μA**). For surface modification, 20 μM **dsGAA-8** was used for DPV measurements in 1 mM $Fe(CN)_6^{-3/-4}$ using counter electrode Pt wire, reference electrode Ag/AgCl, and a working electrode = 2 mm **diameter**.

MoS_2 ink (10 cp viscosity), which remained stable and dispersed even after eight months of storage at room temperature.[41] The TEM image in Figure 1b shows the irregularly shaped flakes of MoS_2 in the ink having an average size of particles ∼316 nm by the longest dimension of the flakes. The inset of Figure 1b shows a single MoS_2 particle in the ink with the measurement of its longest dimension. The inset image also reveals that the exfoliated flakes are few-layered MoS_2 nanosheets, which were also confirmed by optical methods below. The UV−vis characterization shown in Figure 1c confirms the number of layers and optical band gap of the exfoliated MoS_2 ink.[46−49] Several peaks associated with the excitonic transitions in MoS_2 are present in the UV−vis spectrum. Peaks centered at ∼670 nm (1.85 eV) and ∼610 nm (2.03 eV) correspond to adsorption bands of A and B excitons, respectively.[50,51] The energy separation between A and B peaks was used to estimate the number of layers of the exfoliated MoS_2. In this case, the separation value was found to be ∼0.18 eV, corresponding to three and four layers as reported earlier.[49,52,53] Furthermore, a Tauc plot analysis estimated the optical band gap of MoS_2 ink materials. Considering the indirect transitions,[54] a value of optical energy around 1.58 eV was obtained (Figure 1d) confirming three to four layers of MoS_2 in the ink.[55−57] The electrical transport behavior of the MoS_2 ink was studied by monitoring the temperature (T) dependence ($310 < T < 230$) resistance of the MoS_2 ink. The results are consistent with the thermally activated Arrhenius type transport mechanism, which is typical of semiconducting materials (Figure 1e).

Then, the electrochemical activity of inkjet-printed MoS_2 nanosheets on ITO substrate (2 mm dia.) was investigated by cyclic voltammetry in a 1 mM $Fe(CN)_6^{-3/-4}$ solution at a 200 mV/s scan rate (Figure 2a). The bare ITO shows a wide peak separation of ΔE_p = 556 mV and a significantly low peak current of ∼10 μA. However, after printing 2D MoS_2 on ITO, the modified MoS_2/ITO surface showed a significantly reduced peak separation of ΔE_p = 255 mV and high peak currents of ∼28 μA, which confirmed the relatively faster electrode kinetics on the MoS_2 surface. The electrochemical activity was further investigated at a wide range of scan rates between 50−500 mV/s. The electrocatalytic property of the MoS_2-modified surface was found to be superior to the unmodified ITO surface (Figure 2b) where the voltammetric peak current of the MoS_2/ITO surface is higher in intensity and has a twofold higher slope than the unmodified surface. To test the electrocatalytic response of the adsorption of DNA on MoS_2/ITO, a 5 μL aliquot of 20 μM dsGAA-8 was incubated for 16 h followed by measuring the current through differential pulse voltammetry (DPV) in the presence of 1 mM $Fe(CN)_6^{-3/-4}$. The incubation time was optimized by incubating the MoS_2/ITO surface with dsGAA for a 4−20 h time period as shown in Figure S1, where the current was found slightly decreased in the first 4 h and gradually increased with the maximum current obtained at 16 h. The current was steeply decreased when incubated for 20 h, which may be due to the layer-by-layer adsorption of DNA leading to hindering charge transport across the interface. Previous electrochemical studies relied on air drying of the DNA samples for adsorption on the MoS_2 surface.[25,58] Such strategy might have been adopted to overcome the electrostatic repulsion between MoS_2 and DNA. We used a high ionic strength condition, as mentioned previously,[24] to facilitate the adsorption of the DNA on MoS_2 and incubated the samples at 4 °C in a sealed humid container to prevent evaporation. Figure 2c shows the electrocatalytic current following the adsorption of dsGAA-8 on bare ITO and MoS_2/ITO surfaces. It confirms the adsorption of dsGAA on both surfaces under high ionic strengths because both surfaces are negatively charged, and high ionic strength neutralizes the negative charge and facilitates dsGAA adsorption. However, the current enhancement on the MoS_2/ITO surface following the dsGAA adsorption is 1.8-fold higher than the current of dsGAA adsorption on bare ITO. Overall, a 3-fold enhancement in the current was observed on the ITO substrate after the modification of dsGAA/MoS_2. These results corroborated the superior electrochemical performance of the MoS_2 ink with and without DNA modification, which led us to use the ink for flexible device fabrication.

Fabrication of biosensors on chip using desktop tools and flexible substrates has gained popularity due to the ease of fabrication, low-cost mass production, and potential applications in point-of-care testings.[59,60] Wax-on-plastic platforms belong to a new family of flexible devices that have recently emerged and are being used for a variety of applications.[61−63] We fabricated MoS_2-modified wax-on-plastic electrochemical devices for CGG repeat detection using a previously reported

https://dx.doi.org/10.1021/acsami.0c14912
ACS Appl. Mater. Interfaces 2020, 12, 52156−52165

procedure with two modifications.[43] First, we replaced the hand painting of the silver layer with inkjet printing of the AgNP layer. Second, the working electrode was modified by 2D MoS_2 ink via simple drop-casting.[43] As illustrated in Figure 3a, the device fabrication relies on simple solid wax printing on a PET substrate to draw a template for a three-electrode device

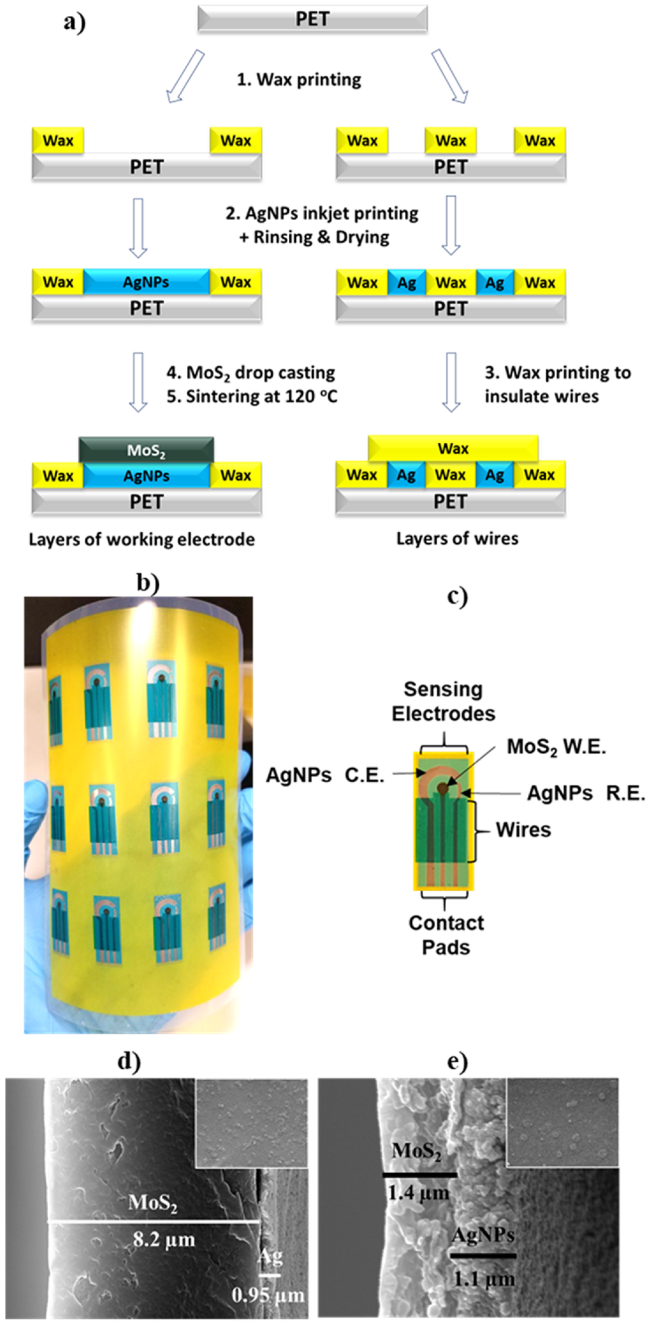

Figure 3. (a) Fabrication scheme showing layers of working electrodes and wire of MoS_2-modified wax-on-plastic platforms; (b) photo shows twelve devices printed on a 6″ × 4″ flexible PET substrate; (c) the image shows parts of the device, i.e., three-electrode sensing electrodes with a 2 mm diameter MoS_2-modified working electrode (W.E.), AgNPs counter (C.E.), AgNPs pseudo-reference (R.E.), wires covered with wax layer, and contact pads at the bottom; (d) an SEM image of MoS_2/AgNP layers before sintering; (e) an SEM image of MoS_2/AgNP layers after sintering. The inset in (d) & (e) shows the topical image of MoS_2 before and after sintering.

(step 1). Then, a silver conductive layer was laid down into the hydrophilic regions of the plastic substrate by inkjet printing of AgNPs (step 2). After washing the silver **nano** particles on top of the wax layer and air drying, a second layer of wax was printed to selectively cover the wires but keep the electrodes and contact pads of the device exposed (step 3). Finally, 4 μL of MoS_2 was drop-casted on top of the working electrode (step 4) and sintered at 120 °C in an Ar environment for 30 min (step 5). There were 12 devices fabricated on each PET substrate sized 6″ × 4″ (Figure 3b). Each device comprises three-electrode sensors with a 2 mm diameter MoS_2-modified working electrode (W.E.), AgNP counter (C.E.), AgNP pseudo-reference (R.E.), wires covered with wax layer, and contact pads at the bottom (Figure 3c). The sintering step in an Ar environment is a crucial step to enhance the electrical/electrochemical conductivity of MoS_2 ink by evaporating solvents and the ethyl cellulose matrix as described previously.[41] The scanning electron microscopic images indicate the device layers and thicknesses before and after the sintering step. Figure 3d shows the thicknesses of MoS_2 (8.2 ± 1.4 μm) and Ag (0.95 ± 0.1 μm) layers before sintering, while Figure 3e shows the change in layer thicknesses after the sintering step with MoS_2 = 1.4 ± 0.1 μm and AgNPs = 1.1 ± 0.1 μm. The significant reduction in the thickness of MoS_2 is due to the evaporation of solvent and volatile additives in the ink, which was also expected for the AgNP layer previously.[43] To find the actual change in the AgNP thickness, we measured the thickness in the absence of MoS_2 layer, which was found to be decreased from 2.4 ± 0.3 μm to 1.4 ± 0.4 μm after sintering as shown in the SEM images in Figure S2a,b (see the Supplementary Information), respectively. Perhaps the thick layer of MoS_2 masked the true thickness of the AgNP layer. In addition, the SEM images also confirmed that the layers are well adhered with each other and with the substrate. The topical view of the MoS_2 electrode shown in the inset images shows the insignificant topical change after the sintering process. Furthermore, elemental compositions of the unmodified AgNP and MoS_2/AgNP surfaces were confirmed following sintering using energy-dispersive X-ray spectroscopy (EDS). Figures S3 and S4 in the Supplementary Information show elemental composition of the unmodified AgNP layer and MoS_2/AgNPs electrode surfaces, respectively. The analysis of AgNPs confirms the high percentage of Ag (78.28%) and absence of Mo and S atoms. Meanwhile, the EDS analysis of the MoS_2/AgNP nearly confirms the 1:2 ratio between Mo and S atoms in the composition with Mo = 11.05% and S = 19.48%. Note: the metal deposition film to prepare the samples contains Au, Pd, and Ag atoms. Electrochemical performance of the MoS_2/AgNPs was tested by measuring the DPV current in the presence 1 mM $Fe(CN)_6^{-3/-4}$. To make the MoS_2 jetable through nozzles, its composition was set to 6% to achieve the required viscosity of 10 cp. However, an intriguing question was how the amount of MoS_2 nanosheets may affect the electrochemical performance. To address this question, we deposited different volumes of the ink from 0.5−4.0 μL on AgNP working electrodes followed by DPV current measurement in the presence of 1 mM $Fe(CN)_6^{-3/-4}$. Figure S5 shows the current response with respect to volume of the deposited MoS_2, where the current was found linearly increasing with the volume of the ink. We used 4.0 μL of 6% MoS_2 to fabricate the devices for the rest of the study as it was the maximum volume that can be hold by the working electrode area. The devices were tested over the course of a two month time period while

https://dx.doi.org/10.1021/acsami.0c14912
ACS Appl. Mater. Interfaces 2020, 12, 52156−52165

kept in a dry container at room temperature. The current responses presented in Figure S6 confirm that the devices can be stored for longer period while kept in dry ambient conditions.

Electrocatalysis via DNA-mediated charge transport has been extensively studied and applied for the detection of lesions and mismatches in nonrepetitive DNA sequences.[64] Recent examples have shown conversion of irreversible electrode kinetics of paracetamol to a quasi-reversible system[65] and sequence-directed electrocatalytic reduction of ferricyanide at DNA-modified gold electrodes.[66] Such interfacial charge transport property of DNA may be characterized as overlapping of the DNA base pair π-stacks with that of the interfacing materials.[64] In this study, we detected the CGG associated with FXS/FXTAS disease via the DNA-mediated electrocatalytic current on 2D MoS_2-modified electrodes. The CGG sequences were simply adsorbed on the MoS_2 surface followed by measuring the current in the presence of the $Fe(CN)_6^{-3/-4}$ probe using the DPV technique. The current measured on the MoS_2/AgNP electrode system was three orders of magnitude higher than the MoS_2/ITO system despite the same area of working electrodes used in both systems, i.e., 2 mm **diameter**. We attribute this current enhancement to the high conductivity of the AgNP base layer, which perhaps substantially reduces potential drop (iR drop) and facilitates the current flow. Figure 4 shows the typical voltammograms

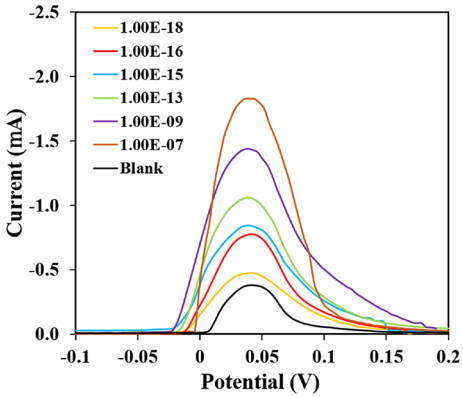

Figure 4. Representative differential pulse voltammetric curves of dsCGG-8 repeats from 1 aM−100 nM concentrations.

recorded for the **ds**CGG-8 repeats in the concentration range of 1 aM−100 nM. The calibration curve shown in Figure 5 confirms a linear correlation between the electrocatalytic current signal and the concentrations with a correlation coefficient of $R^2 = 0.992$. The detection limit signal, LOD_y, was obtained using LOD_y = (blank signal + 3*SD_{blank}) − intercept; where blank signal = 0.4 mA, while three times the standard deviation of blank (3*SD_{blank}) = 0.15 mA. Then, the limit of detection concentration, LOD_x, was determined as 3.0 aM by calculating antilog (LOD_y ÷ sensitivity), where sensitivity is the slope of the calibration curve. The proportional increase in the current with concentration suggests that the increase in interaction between the dsCGG-8 bases and the MoS_2 surface leads to the increase in catalytic current flow, which may also transduce the number of repeats in a sequence at a particular concentration. Therefore, the electrocatalytic current response with respect to repeat length was measured by adsorbing 5−30 repeat units of dsCGG at a 10 aM concentration prepared in Tris buffer containing 100 mM $MgCl_2$ (pH 8.5). As shown in Figure 5b, the electrocatalytic current increased with the repeat length, which indicates that the pathogenic lengths of CGG repeats may respond with a significantly higher current than the normal lengths. For proof-of-concept application, real-to-life samples of dsCGG repeats were isolated from plasmids (see details in the Supplementary Information, Figures S7 and S8) and allowed to adsorb on the MoS_2 surface using the optimized condition. The current responses of the normal length of 26 repeats corresponding FXTAS(-ve) and pathogenic length of 100 repeats corresponding FXTAS(+ve) are shown in Figure 5c. The results confirm that the increase in length leads to the self-amplified current response and can be used to distinguish the normal and abnormal repeat lengths. In the literature, electrochemical detection of DNA hybridization on MoS_2 surfaces relied on desorption of duplexes following the hybridization event for signal transduction, which stems from the previously established assumption that double-stranded DNA has lower affinity for an MoS_2 surface.[25,58] In addition, those studies also applied a negative potential to reinforce the desorption of the formed duplexes. Here, we used the high cationic strength buffer containing 200 mM Na^+ and 20 mM Mg^{2+} to test the affinity of various sequences for MoS_2 surface. A number of sequences having same length, including a single-stranded CGG sequence, double-stranded (CGG, CTG, CAG, and GAA) sequences, and a 1:1 mixture of a noncomplementary CGG/TTC sequence, were allowed to adsorb on MoS_2 using 20 μM concentrations. The purpose of using the high concentration of TNR was to saturate the MoS_2 surface assuming that the difference between the sequences will be undetectable at a very high concentration. Meanwhile, the high ionic strength will keep the duplexes adsorbed on MoS_2 by screening the negative charge of DNA and MoS_2 as described previously.[24] The results shown in Figure 5d compare the current responses of these sequences. Comparing ssCGG-8 and dsCGG-8, the results prove that duplex conformation can remain adsorbed on MoS_2 following hybridization while enhancing the electrocatalytic current. The statistical difference between the means of ssCGG-8 and dsCGG-8 by performing a pooled t test because of two standard deviations are not significantly different. The $t_{calculated}$ for 4 degrees of freedom was found to be 33.931, which is higher than t_{table} = 2.776 at a 95% confidence level. Since $t_{calculated} > t_{table}$, therefore, there is a significant difference between the means of ssCGG-8 and dsCGG-8. Such behavior may be useful for label-free detection through surface hybridization (*vide infra*). The noncomplementary mixture of CGG-8/TTC-8 (20 μM:20 μM) shows a response even lower than ssCGG-8 (20 μM), which proves that the mere presence of a high number of single strands on the surface does not translate into an enhanced electrocatalytic activity. We assume that the presence of TTC-8 interfered with the adsorption of ssCGG-8 on the MoS_2 surface. The significantly different responses of dsCGG-8 (20 μM) and the noncomplementary mixture of CGG-8/TTC-8 (20 μM:20 μM) further verify that the higher catalytic current should be expected from ds-TNR despite the large quantity of single-stranded TNR present on the surface in case of CGG-8/TTC-8. Comparing dsCGG-8 with other double-stranded sequences (dsCTG, dsCAG, and dsGAA) having same concentrations, the statistically different current response of dsCGG-8 after the pooled t test validates the specificity of MoS_2 for the CGG sequence.

Considering the difference in the current response of ssCGG and dsCGG, the potential of CGG detection through surface

https://dx.doi.org/10.1021/acsami.0c14912
ACS Appl. Mater. Interfaces 2020, 12, 52156−52165

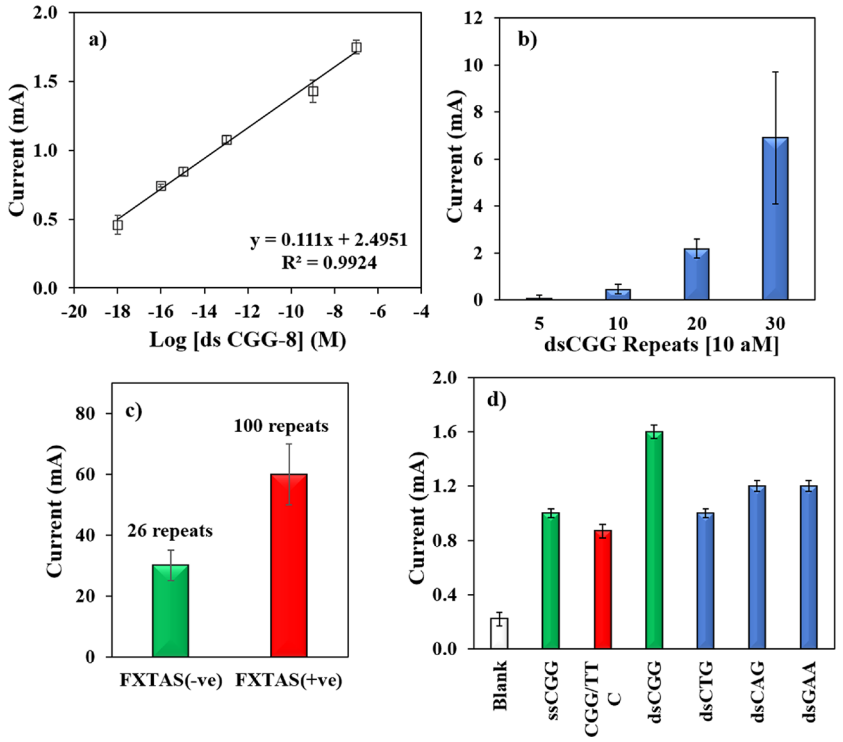

Figure 5. (a) Calibration curve extracted from the peak current shown in Figure 4. (b) Electrocatalytic current response of varying lengths of dsCGG repeats in a 10 aM concentration. (c) Current response of the plasmid extracted **1pM** normal dsCGG-26 and pathogenic dsCGG-100 sequences linked with FXTAS(-ve) and FXTAS(+ve), respectively. (d) Current response of 20 μM of various sequences adsorbed on the MoS_2 surface. The polarity of the current response was changed to positive for comparison.

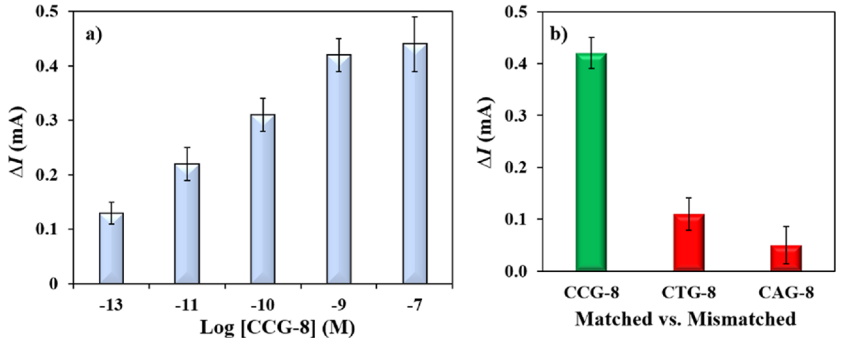

Figure 6. (a) Detection of CCG-8 on MoS_2/AgNP electrodes **fabricated on wax-on-plastic platforms** by surface hybridization at various concentrations of the target. (b) Detection of matched (CCG-8) vs mismatched (CTG-8 and CAG-8) sequences on MoS_2/AgNP electrodes by surface hybridization. ΔI is the change in the current response before and after hybridization.

Table 1. Comparing the Electrochemical Detection Systems Used for CGG Repeat Sequences[a]

repeat	repeat length	technique	label	dynamic range	LOD	strategy	ref
CGG	NR	SWV	CMNPs	NR	NR	use the bifunctional nanoprobe (CMNPs) that is able to bind only to the G−G mismatch DNA and the CGG trinucleotide repeat	12
CGG	10	SWV	$FcNCD_2$	NR	NR	selective binding of the bifunctional probe ($FcNCD_2$) to CGG repeats	67
CGG	10	EIS	NCD/MPA	1 nM−1 μM	NR	selective binding of CGG to the NCD/MPA molecule	68
CGG	5-100	DPV	label-free	1 aM−100 nM	3.0 aM	direct adsorption of dsCGG on the MoS_2 surface.	this work

[a]NR = not reported; LOD = limit of detection; SWV = square wave volatmetry; EIS = electrochemical impedance spectroscopy; DPV = differential pulse voltammetry; CMNPs = carboxyl modified Fe_3O_4 magnetic particles; $FcNCD_2$ = ferrocenyl formamide naphthyridine carbamate dimer; NCD/MPA = naphthyridine carbamate dimer/mercaptopropionic acid.

hybridization was tested by adsorbing a probe sequence, ssCGG-8 (1 μM), on the MoS_2 surface followed by incubating different concentrations of a complementary CCG-8 sequence at room temperature. The change in the electrocatalytic current before and after the hybridization (ΔI) shown in Figure 6a confirms the enhancement in the current signal as a

https://dx.doi.org/10.1021/acsami.0c14912
ACS Appl. Mater. Interfaces 2020, 12, 52156−52165

result of duplex formation with the linear response between the 100 fM and 1 nM target concentration. Thus, CGG hybridization on the MoS_2 surface can also be electrochemically detected without a label as well as without relying on desorption of the duplex in contrary to previous reports.[25,58] To test the specificity of the probe, the ssCGG-8 probe was challenged with 1 nM nonspecific TNR targets CTG-8 and CAG-8, where the current was significantly diminished in the presence of the nonspecific targets as shown in Figure 6b. The results confirm the utility of label-free detection of DNA on the MoS_2 surface using a specific probe sequence that leads to an enhanced electrocatalytic response following the surface hybridization.

Overall, the approach has advantages over previous electrochemical strategies for CGG repeats, summarized in Table 1, that were essentially relying on complex labeling steps and CGG samples in micromolar concentrations,[12,67] using short repeat lengths up to 10 repeats.[68] Moreover, in comparison with the commercial kits for CGG repeats, the LOD (3.0 aM) is equal to 8×10^{-10} ng, while the commercially available test for CGG requires a minimum of 25 ng sample for the test.[69] Hence, the CGG/MoS_2 interfaces are promising for rapid, low-cost, and label-free biosensing platforms for CGG repeats.

CONCLUSION

We demonstrated here the simple, ultrasensitive, and label-free detection of CGG repeats associated with FXTAS on inkjet printable MoS_2 electrodes. The MoS_2-modified inkjet-printed wax-on-plastic devices were found robust, and they showed an enhanced electrocatalytic response with respect to double-stranded conformation, concentration, and length of CGG repeats. The study showed a higher affinity of MoS_2 for CGG repeats compared to other repeat sequences. Moreover, we confirmed that high cationic strength supports electrocatalytic detection of both prehybridized and surface hybridized CGG sequences on MoS_2 surfaces. The limit of detection was found to be 3.0 aM with a 1 aM−100 nM dynamic range for prehybridized CGG repeats. For surface hybridization, the surface adsorbed probe was found to be sensitive at a 100 fM−1 nM concentration range of the CGG target sequence, which showed a significantly diminished response when challenged with nonspecific TNR sequences. Moreover, the high electrocatalytic current was observed for longer repeats along with differential signals from the normal and FXTAS-associated pathogenic lengths of an expanded CGG repeat, which may be helpful in the future to detect very large repeat expansions at even lower concentrations. Although we have utilized the MoS_2 ink in the current study, the bioaffinity of other 2D surfaces (e.g., tungsten disulfide or tin sulfide) may be explored in the future to detect large repeat sequences. The detection method demonstrated here is a step forward toward developing label-free, rapid, sensitive, and cost-effective detection of repeat sequences that can help bring chip-based diagnostics closer to the clinic.

ASSOCIATED CONTENT

Supporting Information

The Supporting Information is available free of charge at https://pubs.acs.org/doi/10.1021/acsami.0c14912.

List of single-stranded and double-stranded TNR sequences (Table S1); DPV current for the incubation time of 20 μM dsGAA on a MoS_2/ITO surface (Figure S1); scanning electron microscopic images of inkjet-printed AgNP layer on a PET substrate (Figure S2); SEM image of AgNP layer and EDS analysis of the AgNPs layer (Figure S3); SEM image of MoS_2 layer and EDS analysis of the MoS_2 layer (Figure S4); effect of the volume of 6% MoS_2 ink deposited on AgNPs on the electrochemical current response (Figure S5); stability test of the MoS_2/AgNP electrodes on wax-on-plastic devices over the course of two months (Figure S6); isolation of CGG repeat-containing DNA fragments;validation of CGG repeat expansion size by plasmid sequencing; sequences of CGG repeat expansion-containing plasmids (Figure S7); and the nucleotide plot and statistics for MinION sequencing of the 100 CGG repeat region of the FMRpolyG GFP pGW2 plasmid (PDF)

(PDF)

AUTHOR INFORMATION

Corresponding Author

Mohtashim H. Shamsi − *Department of Chemistry and Biochemistry, Southern Illinois University, Carbondale, Illinois 62901, United States;* orcid.org/0000-0002-5463-811X; Email: mshamsi@siu.edu

Authors

Narges Asefifeyzabadi − *Department of Chemistry and Biochemistry, Southern Illinois University, Carbondale, Illinois 62901, United States*

Rana Alkhaldi − *Department of Physics, Southern Illinois University, Carbondale, Illinois 62901, United States*

Ahmad Z. Qamar − *Department of Chemistry and Biochemistry, Southern Illinois University, Carbondale, Illinois 62901, United States*

Adrian A. Pater − *Department of Chemistry and Biochemistry, Southern Illinois University, Carbondale, Illinois 62901, United States*

Meera Patwardhan − *Department of Chemistry, Kalamazoo College, Kalamazoo, Michigan 62901, United States*

Keith T. Gagnon − *Department of Chemistry and Biochemistry and Department of Biochemistry and Molecular Biology, School of Medicine, Southern Illinois University, Carbondale, Illinois 62901, United States;* orcid.org/0000-0002-5868-675X

Saikat Talapatra − *Department of Physics, Southern Illinois University, Carbondale, Illinois 62901, United States*

Complete contact information is available at: https://pubs.acs.org/10.1021/acsami.0c14912

Author Contributions

$^{\perp}$N.A. and R.A. contributed equally to this work.

Notes

The authors declare no competing financial interest.

ACKNOWLEDGMENTS

We thank Peter K. Todd (University of Michigan) for sharing plasmids containing 26 and 100 CGG repeat expansions. This work was supported by an NSF EAGER grant #1940716 to M.H.S., an NSF REU grant to support M.P.'s research at SIUC, and an NIH R15 grant to K.T.G.

REFERENCES

(1) Rohilla, K. J.; Gagnon, K. T. RNA Biology of Disease-Associated Microsatellite Repeat Expansions. *Acta Neuropathol. Commun.* **2017**, *5*, 63.

(2) Fu, Y.-H.; Kuhl, D. P. A.; Pizzuti, A.; Pieretti, M.; Sutcliffe, J. S.; Richards, S.; Verkert, A. J. M. H.; Holden, J. J. A.; Fenwick, R. G., Jr.; Warren, S. T.; Oostra, B. A.; Nelson, D. L.; Caskey, C. T. Variation of the CGG Repeat at the Fragile X Site Results in Genetic Instability: Resolution of the Sherman Paradox. *Cell* **1991**, *67*, 1047−1058.

(3) Buermans, H. P. J.; den Dunnen, J. T. Next Generation Sequencing Technology: Advances and Applications. *Biochim. Biophys. Acta, Mol. Basis Dis.* **2014**, *1842*, 1932−1941.

(4) Orr, H. T.; Zoghbi, H. Y. Trinucleotide Repeat Disorders. *Annu. Rev. Neurosci.* **2007**, *30*, 575−621.

(5) van Blitterswijk, M.; Dejesus-Hernandez, M.; Rademakers, R. How Do *C9ORF72* Repeat Expansions Cause Amyotrophic Lateral Sclerosis and Frontotemporal Dementia: Can We Learn From Other Noncoding Repeat Expansion Disorders? *Curr. Opin. Neurol.* **2012**, *25*, 689−700.

(6) Zhao, X.-N.; Usdin, K. The Repeat Expansion Diseases: The Dark Side of DNA Repair. *DNA Repair* **2015**, *32*, 96−105.

(7) Chen, L.; Hadd, A.; Sah, S.; Filipovic-Sadic, S.; Krosting, J.; Sekinger, E.; Pan, R.; Hagerman, P. J.; Stenzel, T. T.; Tassone, F.; Latham, G. J. An Information-Rich CGG Repeat Primed PCR that Detects the Full Range of Fragile X Expanded Alleles and Minimizes the Need for Southern Blot Analysis. *J. Mol. Diagn.* **2010**, *12*, 589−600.

(8) Narzisi, G.; Schatz, M. C. The Challenge of Small-Scale Repeats for Indel Discovery. *Front. Bioeng. Biotechnol.* **2015**, *3*, 8.

(9) Loomis, E. W.; Eid, J. S.; Peluso, P.; Yin, J.; Hickey, L.; Rank, D.; Mccalmon, S.; Hagerman, R. J.; Tassone, F.; Hagerman, P. J. Sequencing the Unsequenceable: Expanded CGG-Repeat Alleles of the Fragile X Gene. *Genome Res.* **2013**, *23*, 121−128.

(10) Akimoto, C.; Volk, A. E.; van Blitterswijk, M.; van den Broeck, M.; Leblond, C. S.; Lumbroso, S.; Camu, W.; Neitzel, B.; Onodera, O.; van Rheenen, W.; Pinto, S.; Weber, M.; Smith, B.; Proven, M.; Talbot, K.; Keagle, P.; Chesi, A.; Ratti, A.; van der Zee, J.; Alstermark, H.; Birve, A.; Calini, D.; Nordin, A.; Tradowsky, D. C.; Just, W.; Daoud, H.; Angerbauer, S.; Dejesus-Hernandez, M.; Konno, T.; Lloyd-Jani, A.; de Carvalho, M.; Mouzat, K.; Landers, J. E.; Veldink, J. H.; Silani, V.; Gitler, A. D.; Shaw, C. E.; Rouleau, G. A.; van den Berg, L. H.; Van Broeckhoven, C.; Rademakers, R.; Andersen, P. M.; Kubisch, C. A Blinded International Study on the Reliability of Genetic Testing for GGGGCC-Repeat Expansions in *C9orf72* Reveals Marked Differences in Results Among 14 Laboratories. *J. Med. Genet.* **2014**, *51*, 419−424.

(11) Liu, Y.; Li, J.; Chang, G.; Zhu, R.; He, H.; Zhang, X.; Wang, S. A Novel Electrochemical Method Based on Screen-Printed Electrodes and Magnetic Beads for Detection of Trinucleotide Repeat Sequence $d(CAG)_n$. *New J. Chem.* **2018**, *42*, 9757−9763.

(12) Zhu, X.; Li, J.; Lv, H.; He, H.; Liu, H.; Zhang, X.; Wang, S. Synthesis and Characterization of a Bifunctional Nanoprobe for CGG Trinucleotide Repeat Detection. *RSC Adv.* **2017**, *7*, 36124−36131.

(13) Li, J.; Liu, Y.; Zhu, X.; Chang, G.; He, H.; Zhang, X.; Wang, S. A Novel Electrochemical Biosensor Based on a Double-Signal Technique for $d(CAG)_n$ Trinucleotide Repeats. *ACS Appl. Mater. Interfaces* **2017**, *9*, 44231−44240.

(14) Fojta, M.; Havran, L.; Vojtiskova, M.; Palecek, E. Electrochemical Detection of DNA Triplet Repeat Expansion. *J. Am. Chem. Soc.* **2004**, *126*, 6532−6533.

(15) Fojta, M.; Brázdilová, P.; Cahová, K.; Pečinka, P. A Single-Surface Electrochemical Biosensor for the Detection of DNA Triplet Repeat Expansion. *Electroanalysis* **2006**, *18*, 141−151.

(16) Yang, I. V.; Thorp, H. H. Modification of Indium Tin Oxide Electrodes with Repeat Polynucleotides: Electrochemical Detection of Trinucleotide Repeat Expansion. *Anal. Chem.* **2001**, *73*, 5316−5322.

(17) Taki, M.; Rohilla, K. J.; Barton, M.; Funneman, M.; Benzabeh, N.; Naphade, S.; Ellerby, L. M.; Gagnon, K. T.; Shamsi, M. H. Novel Probes for Label-Free Detection of Neurodegenerative GGGGCC Repeats Associated with Amyotrophic Lateral Sclerosis. *Anal. Bioanal. Chem.* **2019**, *411*, 6995−7003.

(18) Asefifeyzabadi, N.; Taki, M.; Funneman, M.; Song, T.; Shamsi, M. H. Unique Sequence-Dependent Properties of Trinucleotide Repeat Monolayers: Electrochemical, Electrical, and Topographic Characterization. *J. Mater. Chem. B* **2020**, *8*, 5225−5233.

(19) Kukkar, M.; Mohanta, G. C.; Tuteja, S. K.; Kumar, P.; Bhadwal, A. S.; Samaddar, P.; Kim, K.-H.; Deep, A. A Comprehensive Review on Nano-Molybdenum Disulfide/DNA Interfaces as Emerging Biosensing Platforms. *Biosen. Bioelectron.* **2018**, *107*, 244−258.

(20) Vilian, A. E.; Dinesh, B.; Kang, S.-M.; Krishnan, U. M.; Huh, Y. S.; Han, Y.-K. Recent Advances in Molybdenum Disulfide-Based Electrode Materials for Electroanalytical Applications. *Microchim. Acta* **2019**, *186*, 203.

(21) Zhu, C.; Zeng, Z.; Li, H.; Li, F.; Fan, C.; Zhang, H. Single-Layer MoS_2-Based Nanoprobes for Homogeneous Detection of Biomolecules. *J. Am. Chem. Soc.* **2013**, *135*, 5998−6001.

(22) Loo, A. H.; Bonanni, A.; Ambrosi, A.; Pumera, M. Molybdenum Disulfide (MoS_2) Nanoflakes as Inherently Electroactive Labels for DNA Hybridization Detection. *Nanoscale* **2014**, *6*, 11971−11975.

(23) Wang, X.; Nan, F.; Zhao, J.; Yang, T.; Ge, T.; Jiao, K. A Label-Free Ultrasensitive Electrochemical DNA Sensor Based on Thin-Layer MoS_2 Nanosheets with High Electrochemical Activity. *Biosens. Bioelectron.* **2015**, *64*, 386−391.

(24) Lu, C.; Liu, Y.; Ying, Y.; Liu, J. Comparison of MoS_2, WS_2, and Graphene Oxide for DNA Adsorption and Sensing. *Langmuir* **2017**, *33*, 630−637.

(25) Chu, Y.; Cai, B.; Ma, Y.; Zhao, M.; Ye, Z.; Huang, J. High Sensitive Electrochemical Detection of Circulating Tumor DNA Based on The Thin-Layer MoS_2/Graphene Composites. *RSC Adv.* **2016**, *6*, 22673−22678.

(26) Wang, T.; Zhu, R.; Zhuo, J.; Zhu, Z.; Shao, Y.; Li, M. Direct Detection of DNA Below Ppb Level Based on Thionin-Functionalized Layered MoS_2 Electrochemical Sensors. *Anal. Chem.* **2014**, *86*, 12064−12069.

(27) Heckl, W. M.; Smith, D. P.; Binnig, G.; Klagges, H.; Hänsch, T. W.; Maddocks, J. Two-Dimensional Ordering of The DNA Base Guanine Observed by Scanning Tunneling Microscopy. *Proc. Natl. Acad. Sci.* **1991**, *88*, 8003−8005.

(28) Moses, P. G.; Mortensen, J. J.; Lundqvist, B. I.; Nørskov, J. K. Density Functional Study of the Adsorption and van Der Waals Binding of Aromatic and Conjugated Compounds on the Basal Plane of MoS_2. *J. Chem. Phys.* **2009**, *130*, 104709.

(29) Li, B. L.; Zou, H. L.; Lu, L.; Yang, Y.; Lei, J. L.; Luo, H. Q.; Li, N. B. Size-Dependent Optical Absorption of Layered MoS_2 and DNA Oligonucleotides Induced Dispersion Behavior for Label-Free Detection of Single-Nucleotide Polymorphism. *Adv. Funct. Mater.* **2015**, *25*, 3541−3550.

(30) Vovusha, H.; Sanyal, B. Adsorption of Nucleobases on 2D Transition-Metal Dichalcogenides and Graphene Sheet: A First Principles Density Functional Theory Study. *RSC Adv.* **2015**, *5*, 67427−67434.

(31) Sharma, M.; Kumar, A.; Ahluwalia, P. K. Optical Fingerprints and Electron Transport Properties of DNA Bases Adsorbed on Monolayer MoS_2. *RSC Adv.* **2016**, *6*, 60223−60230.

(32) Ge, J.; Ou, E.-C.; Yu, R.-Q.; Chu, X. A Novel Aptameric Nanobiosensor Based on the Self-Assembled DNA−MoS_2 Nanosheet Architecture for Biomolecule Detection. *J. Mater. Chem. B* **2014**, *2*, 625−628.

(33) Zhang, Y.; Zheng, B.; Zhu, C.; Zhang, X.; Tan, C.; Li, H.; Chen, B.; Yang, J.; Chen, J.; Huang, Y.; Wang, L.; Zhang, H. Single-Layer Transition Metal Dichalcogenide Nanosheet-Based Nanosensors for Rapid, Sensitive, and Multiplexed Detection of DNA. *Adv. Mater.* **2015**, *27*, 935−939.

(34) Li, F.; Huang, Y.; Yang, Q.; Zhong, Z.; Li, D.; Wang, L.; Song, S.; Fan, C. A Graphene-Enhanced Molecular Beacon for Homogeneous DNA Detection. *Nanoscale* **2010**, *2*, 1021−1026.

https://dx.doi.org/10.1021/acsami.0c14912
ACS Appl. Mater. Interfaces 2020, 12, 52156−52165

(35) Lu, C.-H.; Li, J.; Liu, J.-J.; Yang, H.-H.; Chen, X.; Chen, G.-N. Increasing the Sensitivity and Single-Base Mismatch Selectivity of the Molecular Beacon Using Graphene Oxide as the "Nanoquencher". *Chem. – A Eur. J.* **2010**, *16*, 4889–4894.
(36) Liu, K.; Feng, J.; Kis, A.; Radenovic, A. Atomically Thin Molybdenum Disulfide Nanopores with High Sensitivity for DNA Translocation. *ACS Nano* **2014**, *8*, 2504–2511.
(37) Schneider, G. F.; Kowalczyk, S. W.; Calado, V. E.; Pandraud, G.; Zandbergen, H. W.; Vandersypen, L. M. K.; Dekker, C. DNA Translocation Through Graphene Nanopores. *Nano Lett.* **2010**, *10*, 3163–3167.
(38) Coleman, J. N.; Lotya, M.; O'Neill, A.; Bergin, S. D.; King, P. J.; Khan, U.; Young, K.; Gaucher, A.; De, S.; Smith, R. J.; Shvets, I. V.; Arora, S. K.; Stanton, G.; Kim, H.-Y.; Lee, K.; Kim, G. T.; Duesberg, G. S.; Hallam, T.; Boland, J. J.; Wang, J. J.; Donegan, J. F.; Grunlan, J. C.; Moriarty, G.; Shmeliov, A.; Nicholls, R. J.; Perkins, J. M.; Grieveson, E. M.; Theuwissen, K.; Mccomb, D. W.; Nellist, P. D.; Nicolosi, V. Two-Dimensional Nanosheets Produced by Liquid Exfoliation of Layered Materials. *Science* **2011**, *331*, 568–571.
(39) Smith, R. J.; King, P. J.; Lotya, M.; Wirtz, C.; Khan, U.; De, S.; O'Neill, A.; Duesberg, G. S.; Grunlan, J. C.; Moriarty, G.; Chen, J.; Wang, J.; Minett, A. I.; Nicolosi, V.; Coleman, J. N. Large-Scale Exfoliation of Inorganic Layered Compounds in Aqueous Surfactant Solutions. *Adv. Mater.* **2011**, *23*, 3944–3948.
(40) Secor, E. B.; Prabhumirashi, P. L.; Puntambekar, K.; Geier, M. L.; Hersam, M. C. Inkjet Printing of High Conductivity, Flexible Graphene Patterns. *J. Phy. Chem. Lett.* **2013**, *4*, 1347–1351.
(41) Seo, J.-W. T.; Zhu, J.; Sangwan, V. K.; Secor, E. B.; Wallace, S. G.; Hersam, M. C. Fully Inkjet-Printed, Mechanically Flexible MoS_2 Nanosheet Photodetectors. *ACS Appl. Mater. Interfaces* **2019**, *11*, 5675–5681.
(42) Sim, D. M.; Kim, M.; Yim, S.; Choi, M.-J.; Choi, J.; Yoo, S.; Jung, Y. S. Controlled Doping of Vacancy-Containing Few-Layer MoS_2 *via* Highly Stable Thiol-Based Molecular Chemisorption. *ACS Nano* **2015**, *9*, 12115–12123.
(43) Chen, S.; Qamar, A. Z.; Asefifeyzabadi, N.; Funneman, M.; Taki, M.; Elliot, L.; Kinsel, M. E.; Kinsel, G. R.; Shamsi, M. H. Hand-Fabricated CNT/AgNPs Electrodes Using Wax-on-Plastic Platforms for Electro-Immunosensing Application. *Sci. Rep.* **2019**, *9*, 1–9.
(44) Shamsi, M. H.; Kraatz, H.-B. The Effects of Oligonucleotide Overhangs on the Surface Hybridization in DNA Films: An Impedance Study. *Analyst* **2011**, *136*, 3107–3112.
(45) Liang, Y. T.; Hersam, M. C. Highly Concentrated Graphene Solutions via Polymer Enhanced Solvent Exfoliation and Iterative Solvent Exchange. *J. Am. Chem. Soc.* **2010**, *132*, 17661–17663.
(46) Eda, G.; Yamaguchi, H.; Voiry, D.; Fujita, T.; Chen, M.; Chhowalla, M. Photoluminescence from Chemically Exfoliated MoS_2. *Nano Lett.* **2011**, *11*, 5111–5116.
(47) Beal, A. R.; Knights, J. C.; Liang, W. Y. Transmission Spectra of Some Transition Metal Dichalcogenides. II. Group VIA: Trigonal Prismatic Coordination. *J. Phys. C: Solid State Phys.* **1972**, *5*, 3540–3551.
(48) Pagona, G.; Bittencourt, C.; Arenal, R.; Tagmatarchis, N. Exfoliated Semiconducting Pure 2H-MoS_2 And 2H-WS_2 Assisted by Chlorosulfonic Acid. *Chem. Commun.* **2015**, *51*, 12950–12953.
(49) Böker, T.; Severin, R.; Müller, A.; Janowitz, C.; Manzke, R.; Voß, D.; Krüger, P.; Mazur, A.; Pollmann, J. Band Structure of MoS_2, $MoSe_2$, And $\alpha-$ $MoTe_2$: Angle-Resolved Photoelectron Spectroscopy and Ab Initio Calculations. *Phys. Rev. B* **2001**, *64*, 235305.
(50) Molina-Sánchez, A.; Sangalli, D.; Hummer, K.; Marini, A.; Wirtz, L. Effect of Spin-Orbit Interaction on the Optical Spectra of Single-Layer, Double-Layer, and Bulk MoS_2. *Phys. Rev. B* **2013**, *88*, No. 045412.
(51) Cheiwchanchamnangij, T.; Lambrecht, W. R. L. Quasiparticle Band Structure Calculation of Monolayer, Bilayer, and Bulk MoS_2. *Phys. Rev. B* **2012**, *85*, 205302.
(52) Jia, G.; Zhang, Y.; Wang, P. Nano-Photo-Thermal Energy Drive MoS_2/ZNO Nanoheterojunctions Growing. *Opt. Mater. Express* **2016**, *6*, 876–883.
(53) Dhakal, K. P.; Duong, D. L.; Lee, J.; Nam, H.; Kim, M.; Kan, M.; Lee, Y. H.; Kim, J. Confocal Absorption Spectral Imaging of MoS_2: Optical Transitions Depending on the Atomic Thickness of Intrinsic and Chemically Doped MoS_2. *Nanoscale* **2014**, *6*, 13028–13035.
(54) Davis, E. A.; Mott, N. F. Conduction in Non-Crystalline Systems V. Conductivity, Optical Absorption and Photoconductivity in Amorphous Semiconductors. *Philos. Mag.* **1970**, *22*, 0903–0922.
(55) Mak, K. F.; Lee, C.; Hone, J.; Shan, J.; Heinz, T. F. Atomically Thin MoS_2: A New Direct-Gap Semiconductor. *Phys. Rev. Lett.* **2010**, *105*, 136805.
(56) Coehoorn, R.; Haas, C.; Dijkstra, J.; Flipse, C. J. F.; de Groot, R. A.; Wold, A. Electronic Structure of $MoSe_2$, MoS_2, and WSe_2. I. Band-Structure Calculations and Photoelectron Spectroscopy. *Phys. Rev. B* **1987**, *35*, 6195–6202.
(57) Backes, C.; Smith, R. J.; Mcevoy, N.; Berner, N. C.; McCloskey, D.; Nerl, H. C.; O'Neill, A.; King, P. J.; Higgins, T.; Hanlon, D.; Scheuschner, N.; Maultzsch, J.; Houben, L.; Duesberg, G. S.; Donegan, J. F.; Nicolosi, V.; Coleman, J. N. Edge and Confinement Effects Allow *in Situ* Measurement of Size and Thickness of Liquid-Exfoliated Nanosheets. *Nat. Commun.* **2014**, *5*, 4576.
(58) Loo, A. H.; Bonanni, A.; Sofer, Z.; Pumera, M. Transitional Metal/Chalcogen Dependant Interactions of Hairpin DNA with Transition Metal Dichalcogenides, MX_2. *ChemPhysChem* **2015**, *16*, 2304–2306.
(59) Qamar, A. Z.; Shamsi, M. H. Desktop Fabrication of Lab-On-Chip Devices on Flexible Substrates: A Brief Review. *Micromachines* **2020**, *11*, 126.
(60) Chen, S.; Shamsi, M. H. Biosensors-On-Chip: A Topical Review. *J. Micromech. Microeng.* **2017**, *27*, No. 083001.
(61) Qamar, A. Z.; Amar, K.; Kohli, P.; Chowdhury, F.; Shamsi, M. H. Wax Patterned Microwells for Stem Cell Fate Study. *RSC Adv.* **2016**, *6*, 104919–104924.
(62) Qamar, A. Z.; Asefifeyzabadi, N.; Motahareh, T.; Naphade, S.; Ellerby, L. M.; Shamsi, M. H. Characterization and Application of Fluidic Properties of Trinucleotide Repeat Sequences by Wax-on-Plastic Microfluidics. *J. Mater. Chem. B* **2020**, *8*, 743–751.
(63) Qamar, A. Z.; Parker, G.; Kinsel, G. R.; Shamsi, M. H. Evolution of Wax-On-Plastic Microfluidics for Sub-Microliter Flow Dynamics and Its Application in Distance-Based Assay. *Microfluid. Nanofluid.* **2019**, *23*, 81.
(64) Furst, A. L.; Hill, M. G.; Barton, J. K. Electrocatalysis in DNA Sensors. *Polyhedron* **2014**, *84*, 150–159.
(65) Althagafi, I. I.; Kassem, M. A.; Awad, M. I. Enhanced Electrocatalytic Oxidation of Paracetamol at DNA Modified Gold Electrode. *Electroanalysis* **2020**, *32*, 437–444.
(66) Kékedy-Nagy, L.; Shipovskov, S.; Ferapontova, E. E. Electrocatalysis of Ferricyanide Reduction Mediated by Electron Transfer Through the DNA Duplex: Kinetic Analysis by Thin Layer Voltammetry. *Electrochim. Acta* **2019**, *318*, 703–710.
(67) He, H.; Xia, J.; Peng, X.; Chang, G.; Zhang, X.; Wang, Y.; Nakatani, K.; Lou, Z.; Wang, S. Facile Electrochemical Biosensor Based on a New Bifunctional Probe for Label-Free Detection of CGG Trinucleotide Repeat. *Biosens. Bioelectron.* **2013**, *49*, 282–289.
(68) He, H.; Peng, X.; Huang, M.; Chang, G.; Zhang, X.; Wang, S. An Electrochemical Impedance Sensor Based on a Small Molecule Modified Au Electrode for the Recognition of a Trinucleotide Repeat. *Analyst* **2014**, *139*, 5482–5487.
(69) Lim, G. X. Y.; Yeo, M.; Koh, Y. Y.; Winarni, T. I.; Rajan-Babu, I.-S.; Chong, S. S.; Faradz, S. M. H.; Guan, M. Validation of a Commercially Available Test That Enables the Quantification of the Numbers of CGG Trinucleotide Repeat Expansion in *FMR1* Gene. *PLoS One* **2017**, *12*, No. e0173279.

https://dx.doi.org/10.1021/acsami.0c14912
ACS Appl. Mater. Interfaces 2020, 12, 52156–52165